Australian Government
Department of Defence
Defence Science and
Technology Organisation

Simulation of Flow Past a Sphere using the Fluent Code

D.A. Jones and D.B. Clarke

Maritime Platforms Division
Defence Science and Technology Organisation

DSTO-TR-2232

ABSTRACT

We use the commercial computational fluid dynamics code Fluent to simulate the flow around a sphere in several different flow regimes; steady-state laminar flow at a Reynolds number (Re) of 100, time-dependent laminar flow at Re = 300, and turbulent flow at Re = 10^4 and Re = 10^6. These simulations provide a test of the ability of the code to accurately reproduce typical flow structures observed in generic bluff body flows, such as those experienced by submarines and Unmanned Underwater Vehicles (UUVs). The simulations are compared both with experimental results and computations from other computer codes and it is found that Fluent is able to accurately simulate the fluid behaviour in each of the above flow regimes.

Published by

Maritime Platforms Division
DSTO Defence Science and Technology Organisation
506 Lorimer St
Fishermans Bend, Victoria 3207 Australia

Telephone: (03) 9626 7000
Fax: (03) 9626 7999

AR-014-365
December 2008

APPROVED FOR PUBLIC RELEASE

Simulation of Flow Past a Sphere using the Fluent Code

Executive Summary

The use of Computational Fluid Dynamics (CFD) codes to simulate the flow around geometrically complicated shapes such as aeroplanes, cars and ships has become standard engineering practice in the last few years. The computer code Fluent is a commercial CFD code which is used routinely by members of the Hydrodynamics Group within DSTO's Maritime Platforms Division (MPD) to simulate flows relevant to underwater vehicle design and surface ship wakes. In this report we test the ability of the code to accurately simulate the flow around a sphere over a large range of Reynolds numbers (Re). This is a stringent test of the code as it involves a number of very different flow regimes, varying from laminar steady-state flow near Re = 100 to time-dependent turbulent flow at Re = 10^6.

These simulations are also intended to provide a benchmark comparison for the finite difference CFD code Vortel, currently under development at Naval Underwater Warfare Center, Newport, Rhode Island in collaboration with researchers at MPD. Vortel is based on the Lagrangian Vorticity method and offers advantages over commercial CFD codes for the simulation of flow around multiple bodies in relative motion. It has already been used to simulate unmanned undersea vehicle docking manoeuvres, as well as unsteady bow thruster hydrodynamics and the unsteady separated flow fields past an oscillating airfoil.

Four different flow regimes are studied in detail: steady-state laminar flow at Re = 100, time-dependent laminar flow at Re = 300, turbulent flow with laminar boundary layers at Re = 10^4 and turbulent flow with turbulent boundary layers at Re = 10^6. The simulated flows were found to be in excellent agreement with both experimental results, where available, and with the results obtained by other authors using different simulation codes. The simulations described in this report illustrate the capability of the Fluent code to accurately reproduce typical flow structures observed on this generic bluff body flow for both time independent/time-dependent and laminar/turbulent flow regimes.

Authors

David A. Jones
Maritime Platforms Division

Dr. David A. Jones obtained a B.Sc. (Hons) and Ph.D. in Theoretical Physics from Monash University in 1973 and 1976 respectively. He joined the then Materials Research Laboratories in 1983 after postdoctoral positions at the University of Strathclyde, Glasgow; Queen Mary College, London University, and the University of New South Wales, Sydney. During 1987/88 he was a visiting scientist at the Laboratory for Computational Physics and Fluid Dynamics at the Naval Research Laboratory, Washington, DC. He has authored 80 journal articles and technical reports and given more than 60 presentations at scientific meetings. His research has covered a variety of areas including polymer dynamics, the application of chaos theory to atomic and molecular physics, laser-plasma interaction theory, warhead design, air blast, detonation physics and computational fluid dynamics.

David B. Clarke
Maritime Platforms Division

David Clarke commenced work in the Maritime Operations Division (MOD) at AMRL in 1988 after completing a BSc at Sydney University. His work in MOD focused on magnetic sensors and instrumentation. He obtained a Graduate Diploma in computer engineering from RMIT in 1996. In 1998 he joined the Maritime Platforms Division to work on the hydrodynamics of underwater vehicles. His work on underwater vehicles has encompassed experiment, empirical and computational hydrodynamics.

Contents

1. Introduction

The use of computational fluid dynamics codes to simulate the flow around geometrically complicated shapes such as aeroplanes, cars and ships has become standard engineering practice in the last few years. A number of commercially available codes can be used to perform these studies, including the finite volume codes Fluent [11] and CFX [3], both of which are used routinely by the Hydrodynamics Group within DSTO's Maritime Platforms Division (MPD) to perform computational fluid dynamics (CFD) studies on underwater flow problems relevant to underwater vehicle design. The strength of the commercial codes generally lies in their excellent pre-processor software, which allows robust meshes to be constructed around very complicated shapes, and the number of quite advanced turbulence models contained within them. Whilst these codes are now also developing the ability to handle problems with moving and deforming meshes, these features are typically structured around particular geometries of commercial importance, such as piston motion in cylinder blocks, fan blades in cyclones and stores separation from aircraft. The ability to simulate flow around an arbitrary number of bodies in relative motion, which is of interest to the MPD Hydrodynamics Group, is not intrinsically suited to these codes.

One computer code which shows considerable promise in this area is Vortel, a finite difference code currently under development at NUWC, Newport, Rhode Island in collaboration with researchers at MPD [15]. Vortel is based on the Lagrangian Vorticity method [35] and will be used to simulate flow around multiple bodies in relative motion. It has already been used to simulate unmanned undersea vehicle docking manoeuvres [17,18] as well as unsteady bow thruster hydrodynamics [16] and the unsteady separated flow fields past an oscillating airfoil [19]. As part of the development process Vortel is being tested against a number of benchmark problems, one of which is the simulation of the flow past a sphere over a large range of Reynolds numbers (Re). This is a stringent test of the code as it involves a number of different flow regimes, from laminar steady-state flow near Re = 100 to time-dependent turbulent flow at Re = 10^6. To provide verification, the Fluent code has been used to simulate the flow past a sphere in several flow regimes; steady-state laminar flow at Re = 100, time-dependent laminar flow at Re = 300, and turbulent flow at Re = 10^4 and Re = 10^6.

As Fluent is used to perform the majority of the flow simulation studies performed by the Hydrodynamics Group, the computations reported here also provide a timely test of the ability of the code to accurately reproduce typical flow structures observed in generic bluff body flows. The simulations are compared both with experimental results and computations from other computer codes and it is found that Fluent is able to accurately simulate the fluid behaviour in each of the above flow regimes. At Re = 300 the laminar solver in Fluent accurately calculates the regular vortex shedding observed both experimentally and in many numerical simulations, while the new Large Eddy Simulation (LES) turbulence model available in the latest version of Fluent (Fluent 6.3) is shown to be able to simulate the drop in drag coefficient which occurs near Re = 3.8×10^5 due to the transition from laminar to turbulent boundary layer separation. Comparison with the simulation results obtained from the Vortel code are described elsewhere [15].

2. Flow regimes as a function of Reynolds number

The nature of the flow around a sphere changes dramatically as the Reynolds number of the flow increases. In general, the higher the Reynolds number, the more complex the flow. In this section we describe the nature of the flow for different Reynolds numbers in a range between Re = 20 and Re = 1.0×10^6. It should be noted that the Reynolds number range for each of the different flow regimes shows some variation depending on the individual researchers, so that the Reynolds numbers given here delineating one flow regime from another should be considered to have a small amount of uncertainty attached to them.

2.1 Steady axisymmetric regime: 20 < Re < 210

Experimental investigations of the steady wake behind a sphere at low Reynolds numbers have been performed by Taneda [48] and Nakamura [38]. Taneda found that for Reynolds numbers less than 24 the flow around the sphere is perfectly laminar, no flow separation occurs, and the flow on the downstream side of the sphere is identical to that on the upstream side.

Above a Reynolds number of 25 the flow separates from the sphere close to the rear stagnation point and forms a closed recirculating wake in the shape of an axisymmetric vortex ring. As the Reynolds number increases both the separation angle and the length of the wake grow. Taneda showed that the size of the vortex ring was proportional to the logarithm of the Reynolds number and that the flow was stationary up to a Reynolds number of approximately 130, after which oscillations began to appear at the rear of the vortex ring. Nakamura however found that the vortex ring was stable and axisymmetric up to a Reynolds number of approximately 190, and that a stable vortex ring formed at a Reynolds number as low as Re = 7.

Magarvey and Bishop [34] and Wu and Faeth [54] experimentally investigated the flow past a sphere over a larger range of Reynolds numbers and found similar behaviour to that found by Nakamura [38]. Wu and Faeth found that the flow was axisymmetric and stable up to Re = 200, while Magarvey and Bishop found the same behaviour occurring up to Re = 210. These observations are in good agreement with the calculations of Natarajan and Acrivos [39], who investigated the linear stability of the steady axisymmetric flow past a sphere and found that the flow undergoes a regular bifurcation at a Reynolds number of about 210 and results in the development of a non-axisymmetric wake.

2.2 Steady planar-symmetric regime: 210 < Re < 270

Above this transition point near Re = 210 Magarvey and Bishop [34] and Wu and Faeth [54] noted that the flow remained attached and stable but was no longer axisymmetric. The nature of the flow in this regime consists of two streamwise vortical tails of equal strength and opposite sign. Magarvey and Bishop [34] referred to this structure as a double threaded wake and were able to observe and photograph the phenomenon by following the drop of an immiscible fluid in a number of different liquid-liquid systems.

Although the flow no longer possesses axial symmetry the flow still exhibits planar symmetry in the plane containing the two vortical tails. The orientation of this symmetry plane is tilted off the streamwise axis and has been explained by Johnson and Patel [23] as being due to an azimuthal instability of the low pressure core of the wake vortex. The actual orientation of the plane is arbitrary and will be determined by random external influences, such as perturbations due to model supports in an experimental situation, or truncation errors or grid asymmetries in numerical simulations.

The loss of axial symmetry results in the appearance of a lateral (lift) force which is directed in the plane of flow symmetry. The presence of this force was observed by Magarvey and Bishop [34] by noting that the liquid drops in their experiments deviated from a vertical line of fall. More recently the presence of a lateral force has been verified by several numerical simulations. Gushchin *et al*. [14] used an explicit second order finite difference scheme to perform direct numerical simulations of the flow around a sphere and found zero lift force at Re = 210 but a finite value at Re = 210.5. Johnson and Patel [23] found that the simulated lift force jumped by three orders of magnitude between Re = 211 and Re = 212.

Tomboulides and Orszag [50] used direct numerical simulation based on spectral-type methods to simulate the flow between Re = 25 and Re =1000. Their simulations showed that the flow past a sphere is axisymmetric up to a Reynolds number of approximately 212, and that beyond this Reynolds number the flow undergoes a transition to three-dimensionality through a regular bifurcation. The characteristics of the resulting steady flow field, which they found to be stable up to a Reynolds number of approximately 270, corresponded to that of the double-thread wake reported by Magarvey and Bishop [34]. The simulations showed that the double thread wake consisted of two opposite-sign streamwise vortices which extend to infinity and appear in the experiment as two dye threads emanating from the end of the recirculation region.

2.3 Unsteady planar-symmetric regime: 270 < Re < 400

As the Reynolds number increases within this range a transition from the steady planar-symmetric wake to a time-dependent planar-symmetric wake occurs. The unsteadiness first appears as a waviness in the double threaded wake. This form of instability in the wake exists only over a very limited large of Reynolds numbers, between Re = 270 and Re = 290. Above Re = 290 Magarvey and Bishop [34] found that the wake became unsteady and consisted of a series of interconnected vortex loops, while Wu and Faeth [54] found that the flow became unsteady and exhibited vortex shedding at a Reynolds number close to 280. Sakamoto and Haniu [43] conducted an extensive series of experiments on the flow past spheres in the Reynolds number range from 300 to 40,000 using hot-wire techniques in a low speed wind tunnel and flow-visualisation techniques in a water channel. They found that hairpin shaped vortices began to be shed periodically at Re = 300 with regularity in strength and frequency and that the planar symmetry of the flow was maintained.

These experimental observations [34, 43, 54] are in broad agreement with a number of recent numerical simulations. Johnson and Patel [23] performed numerical simulations at Re = 270 and found a steady-state solution, while at Re = 280, the next highest Reynolds number considered in their calculations, the solution clearly became periodic. The results of their

simulation at Re = 300 showed a highly organised periodic flow dominated by vortex shedding, with a Strouhal number of 0.137 and a mean value for the drag coefficient C_d of 0.656.

Ploumhans, *et al.* [40] used three-dimensional vortex methods to simulate the flow past a sphere at Reynolds numbers of 300, 500 and 1000. At Re = 300 they found that the flow attained a time periodic regime with a Strouhal number of 0.135 and a mean value for C_d of 0.683. A finite value for the lift coefficient was obtained and the flow exhibited planar symmetry in a plane passing through the wake centre line.

The direct numerical simulations of Tomboulides and Orszag [52] used a mixed spectral element / Fourier spectral method and found that the transition between three-dimensional steady flow with planar symmetry to single frequency periodic flow with vortex shedding occurred in the range between Re = 270 and Re = 285. They also performed a simulation at Re = 300 and found a Strouhal number of 0.136 and a mean drag coefficient of 0.671. They noted that the basic wake structure consisted of a succession of interconnected vortex loops which maintained the planar symmetry observed at lower Reynolds numbers.

Mittal [37] performed numerical simulations of flow past prolate spheroids using a Fourier-Chebyshev spectral collocation method for Reynolds numbers in the range from Re = 50 to Re = 500. At Re = 350 he found that the wake was characterised by the appearance of interconnected vortex loops which were shed from the sphere at a well defined frequency with a Strouhal number of 0.140. Planar symmetry could also be observed in the unsteady wake in a plane passing through the wake centre line.

2.4 Unsteady asymmetric regime: 400 < Re < 1000

In this range the planar symmetry of the flow is eventually lost because the azimuthal location at which the vortex loops are formed changes from cycle to cycle in an irregular fashion. The exact value of the Reynolds number at which this begins to happen is difficult to specify precisely. In the experiments of Sakamoto and Haniu [43] it was noted that the shedding of the vortices started to become irregular near Re = 420 and was completely random at Re = 480. Mittal [36] conducted a series of direct numerical simulations in the range 350 < Re < 425 to more accurately locate the upper extent of the planar symmetric range and found that the wake loses planar symmetry between Re = 350 and Re = 375. The cycle-to-cycle variations in the vortex formation angle at these Reynolds numbers where quite small however and did not become appreciable until Re = 425. Mittal [36] thus explained this apparent discrepancy with the results of Sakamoto and Haniu as being due to the inability of experimental flow visualisation techniques to detect small scale variations in the azimuthal angle of vortex formation. The numerical simulations of Dallmann *et al.* [9] however indicate that planar symmetry still exists in the flow at R = 400.

At Re = 500 the simulations of Tomboulides and Orszag [50] showed a wake structure similar to the one observed at Re = 300, but the vortex loops were shed from the sphere with different orientations, hence the planar symmetry observed at Re = 300 was not preserved. Time spectra of the velocity at several locations showed that the flow had changed from a one-

frequency flow at Re = 300 to an almost chaotic system at Re = 500, although a dominant peak at a Strouhal number of 0.167 could still be observed.

A further transition in the nature of the flow occurs near Re = 800. Above this Reynolds number the measurements of Kim and Durbin [26] showed that two dominant modes of unsteadiness exist in the wake. These are associated with a small scale instability in the separating shear layer (the Kelvin-Helmhotz instability) and a large scale instability in the wake (the vortex shedding). The higher frequency component was only detected in the region immediately downstream of the sphere, leading Kim and Durbin to the conclusion that this mode was due to a Kelvin-Helmhotz instability in the separating shear layer. The Strouhal number associated with vortex shedding was found to be practically independent of Reynolds number for Re > 800 and had a value of approximately 0.2, while the Strouhal number associated with the Kelvin-Helmholtz instability increased with increasing Reynolds number. Similar results have also been found in the experiments of Sakamoto and Haniu [43] and Chomaz *et al*. [4]. The presence of a Kelvin-Helmholtz instability in the separating shear layer above Re = 800 has also been seen in the numerical simulations of Tomboulides and Orszag [50], who used a Spectral Element / Fourier Spectral method.

2.5 Turbulent wake regime: Re > 1000

Taneda [49] made visual observations of the flow past a sphere in a wind tunnel in the range $10^4 < \mathrm{Re} < 10^6$ using a combination of the surface oil flow method, the smoke flow visualisation method and the tuft-grid method. For Reynolds numbers in the range $1.0 \times 10^4 < \mathrm{Re} < 3.8 \times 10^5$ he showed that the wake undergoes a progressive wave motion in a plane containing the streamwise axis. The Strouhal number and drag coefficient remain approximately constant at 0.2 and 0.5 respectively, but the plane containing the oscillations rotates slowly and irregularly around the axis. These observations are in agreement with those of Achenbach [1,2], who found that strong periodic fluctuations existed in the wake right up to the critical Reynolds number of 3×10^5, and that the vortex separation point rotated around the sphere.

Above the critical Reynolds number around $\mathrm{Re} = 3.8 \times 10^5$ the near-wake recirculation region shrinks considerably, the drag coefficient decreases sharply to a value of $C_d \approx 0.08$, and periodic vortex shedding is no longer able to be detected experimentally. The experiments of Taneda [49] show that in the range $3.8 \times 10^5 < \mathrm{Re} < 1.0 \times 10^6$ the sphere wake forms a pair of streamwise line vortices at a short distance from the streamwise axis and the vortex pair rotates slowly and randomly about that axis.

Numerical simulations of flow for Reynolds numbers greater than 10^3 have been performed mainly using Large Eddy Simulation (LES) or Detached Eddy Simulation (DES) techniques, although a few authors have attempted to use either Reynolds Averaged Navier Stokes (RANS) or unsteady Reynolds Averaged Navier Stokes (URANS) methods, with limited success. Drikakis [10] computed the flow past a sphere at Reynolds numbers of 1.62×10^5 and 5×10^6 using both a k-ε model and the Baldwin-Lomax model. Comparison with experiment was limited to plots of pressure coefficient versus polar angle. At the lower Reynolds number the k-ε model gave good agreement with the experimental results prior to the separation point, but limited agreement in the aft region. At the higher Reynolds number the k-ε model

performed poorly for most values of the polar angle. The Baldwin-Lomax model was very inaccurate at both Reynolds numbers.

Constantinescu and Squires [6] simulated the flow over a sphere at Re = 10^4 using URANS, LES and DES techniques. The URANS calculations were performed using the *k*-ε, *k*-ω, V2f and Spalart-Allmaras models. Spatial discretisation was based on generalised curvilinear coordinates and high order finite difference approximations and time advancement was via the fractional step method. With the exception of the two-layer *k*-ε model, which performed poorly everywhere, the URANS predictions of the pressure coefficient and the streamwise drag coefficient were in reasonable agreement with experiment. The URANS simulations however were not able to accurately simulate the drag coefficient and the energy content associated with the main instability modes. Both the LES and DES computations showed the presence of a second high frequency band in the power spectra and the calculated Strouhal numbers for both the low frequency (vortex shedding) and high frequency (Kelvin-Helmholtz instability) modes were in good agreement with the experimental results of Sakomoto and Haniu [43]. None of the URANS simulations [6,10] showed the presence of the higher frequency band.

Constantinescu and Squires [7] simulated the flow over a sphere using DES on a structured hexahedral mesh having 450,000 nodes for Reynolds numbers of 1.0×10^5, 4.2×10^5 and 1.14×10^6. In the subcritical regime (Re = 1.0×10^5) with laminar boundary layer separation DES was able to capture the large scale vortex shedding as well as the formation of the vortex tubes in the separated shear layers due to the growth of Kelvin-Helmholtz instabilities in these layers. Good agreement was found with experimental data for drag coefficient, location of transition on the sphere, and the distribution of pressure and skin-friction coefficients. In the supercritical regime (Re = 4.2×10^5 and 1.14×10^6) DES accurately predicted the position of boundary layer separation and the distribution of the mean pressure coefficient over the sphere surface, but the skin friction coefficient was less accurately predicted. Improved agreement was obtained when the model was activated near the region where transition was observed in experiments.

Kim [29] used LES on unstructured meshes to simulate flow around a sphere for Reynolds numbers of 1.0×10^4 and 1.14×10^6. Two different sub-grid scale stress models were used, a dynamic Smagorinsky model and a localised dynamic kinetic energy model, but there was little difference in the results predicted by the two models. At Re = 1.0×10^4 both models accurately predicted the magnitude of the drag coefficient, the vortex shedding Strouhal number and the separation angle. As Re increased further the magnitude of the drag coefficient was accurately predicted but the locations of the separation point and the onset of the transition from laminar to turbulent flow in the boundary layer were much less satisfactory. A summary of the different flow regimes is contained in Table 1.

Table 1: Summary of different flow regimes as a function of Reynolds number

Re range	Nature of Flow	Drag coefficient	Strouhal number
$20 \leq Re \leq 210$	Steady axisymmetric flow with closed recirculating wake in the shape of a vortex ring.	$2.7 \rightarrow 0.7$	Steady state flow
$210 \leq Re \leq 270$	Flow is attached, stable and consists of two streamwise vortical tails of equal strength and opposite sign. Flow exhibits planar symmetry.	C_d continues to fall monotonically	Steady state flow
$270 \leq Re \leq 300$	Transition to unsteady wake consisting of the periodic shedding of a series of interconnected vortex loops. Flow still exhibits planar symmetry.	Mean value of $C_d \approx 0.66$ - 0.68	$S_t \approx 0.14$
$400 \leq Re \leq 800$	Vortex loops continue to be shed but the azimuthal angle at which they are formed begins to oscillate in an irregular fashion and the planar symmetry is lost.	Mean value falls to 0.5 at Re = 800	S_t slowly increases to 0.2 at Re = 800
$800 \leq Re \leq 3.8 \times 10^5$	Vortex loops continue to be shed but in a more irregular manner, although strong periodic fluctuations still exist in the wake.	$C_d \approx 0.5$ over entire range	$S_t \approx 0.2$ over entire range
$3.8 \times 10^5 \leq Re \leq 1.14 \times 10^6$	Near wake region shrinks considerably, drag decreases sharply, periodic vortex shedding is no longer able to be detected experimentally.	$C_d \approx 0.08$ at the critical point, then slowly rises to ≈ 0.12	Considerable uncertainty exists in the literature

3. The Fluent Code

Fluent is a computational fluid dynamics computer code developed and marketed by Fluent Inc. [11]. The code solves the equations for conservation of mass, momentum, energy and other relevant fluid variables using a cell-centred finite-volume method. First the fluid domain is divided into a large number of discrete control volumes (also known as cells) using a pre-processor code which creates a computational mesh on which the equations can be solved. The meshing software available with Fluent is called Gambit. This software allows the use of several types of computational cells including triangular, quadrilateral, hexahedral, tetrahedral, pyramidal, prismatic and hybrid meshes.

Once the fluid domain has been meshed, the governing equations (in integral form) are applied to each discrete control volume and used to construct a set of non-linear algebraic equations for the discrete dependent variables. Fluent then offers the user a number of choices for the algorithm used to solve these equations, including coupled explicit, coupled implicit, and segregated solvers. In all the calculations reported here only the segregated solver has been used. In this approach the governing equations are solved sequentially. Since these equations are non-linear they are first linearised using an implicit method. This produces a scalar system of equations containing only one equation per computational cell per degree of freedom. A point implicit (Gauss-Siedel) linear equation solver is then used in conjunction with an algebraic multigrid (AMG) method to solve the resultant scalar system of equations for the dependent variable in each cell. Since the equations are non-linear several iterations of the solution loop must be performed before a converged solution is obtained.

3.1 Pressure-Velocity Coupling

Using this approach, an equation for each component of the momentum equation and then the continuity equation are solved sequentially. Once the three components of velocity have been calculated for each cell using this sequential system the velocities may not satisfy the continuity equation and so a "Poisson-type" equation for a pressure correction is derived from the continuity equation and the linearised momentum equations. This pressure correction equation is then solved to obtain the necessary corrections to the pressure and velocity fields such that continuity is satisfied.

Although the pressure variable appears in each of the component momentum equations each of these equations is solved by treating the relevant component of velocity as the unknown variable and the pressure field is taken to be that from the previous iteration. In this sequential procedure the continuity equation is used as an equation for the pressure. However pressure does not appear explicitly in the continuity equation for incompressible flows (which are the only flows considered in this report) and so a procedure must be devised to introduce pressure into this equation. Fluent provides methods based on the SIMPLE (Semi-Implicit Method for Pressure-Linked Equations) family of algorithms to do this.

The basic SIMPLE algorithm uses a relationship between velocity and pressure corrections to enforce mass conservation and to obtain the pressure field. The SIMPLEC algorithm (SIMPLE-Consistent) is a variation of the SIMPLE algorithm which uses a more refined expression for the variable flux through each of the cell faces. The PISO pressure-velocity coupling scheme (Pressure-Implicit with Splitting of Operators) is also part of the SIMPLE family of algorithms and is based on a higher degree of approximation for the relationship between the corrections for pressure and velocity. The PISO algorithm takes more CPU time per solver iteration, but it can dramatically decrease the number of iterations required for convergence, especially for transient problems. The PISO algorithm also allows Fluent to obtain solutions on highly skewed meshes in approximately the same number of iterations as required for more orthogonal meshes.

3.2 Spatial Discretisation

Fluent stores discrete values of the variables at the cell centres, however values of the variables are required at the cell faces for the convection terms in the equations and these must be interpolated from the cell centre values. In Fluent 6.1 this is accomplished using an upwind scheme and there are several alternatives: first-order upwind, second-order upwind, power law, and QUICK.

In the first-order upwind scheme quantities at cell faces are determined by assuming that the cell-centre values of any variable represent a cell-average value and hold throughout the entire cell. Hence the face quantities are identical to the cell quantities. The Power-Law scheme is an improvement which interpolates the face value of a variable by using the exact solution to a one-dimensional convection-diffusion equation. When the flow is dominated by convection this implies that the face value of the variable is effectively equal to the cell value in the upwind direction. If the flow is weak and diffusion stronger then the Power-Law

scheme amounts to a simple linear average of the value of the variable at the current cell location and the upstream cell. The Second-Order Upwind Scheme provides true second order accuracy by performing a Taylor series expansion of the cell-centred solution about the cell centroid. The QUICK scheme also allows calculation of a higher-order value of the convected variable at the cell face by using a weighted average of second-order upwind and central interpolation.

Fluent 6.2 contains enhanced discretisation schemes which have been motivated by the new LES and DES turbulence models available in this version of the code. Because accurate spatial discretisation is crucial in LES version 6.2 of Fluent contains a new second-order central differencing scheme for the discretisation of convective terms. Even higher order upwind-biased schemes such as second-order upwind, QUICK and third-order MUSCL schemes introduce considerable amounts of numerical diffusion. This is particularly detrimental in LES calculations because numerical diffusion, no matter how small, can easily overwhelm physical diffusion. Central differencing schemes are well known to have either very low, or sometimes zero, numerical diffusion, and hence are ideal for LES calculations. This unfortunately can lead to another problem however, in that the lack of any numerical damping can allow unphysical oscillations in the solutions to develop. To overcome this possibility a bounded central differencing scheme was also introduced in version 6.2 of Fluent. This scheme essentially detects any oscillations in the solution field with a wavelength less than twice the local grid spacing. It then suppresses these oscillations by switching to upwind schemes of varying orders, depending on the severity of the oscillations, but only in the regions of space where these oscillations occur. Because of these features, Fluent version 6.2 was used for all the LES simulations described in section 6.

4. Turbulence Models

Turbulent flows are characterised by velocity fields which fluctuate rapidly both in space and time. Since these fluctuations occur over several orders of magnitude it is computationally very expensive to construct a grid which directly simulates both the small scale and high frequency fluctuations for problems of practical engineering significance. Two methods can be used to eliminate the need to resolve these small scales and high frequencies: Reynolds Averaging and Filtering.

4.1 Reynolds Averaging

In the Reynolds Averaged approach all flow variables are divided into a mean component (which can vary slowly in time) and a rapidly fluctuating component and then all equations are time averaged to remove the rapidly fluctuating components. In the Navier-Stokes equation the time averaging introduces new terms which involve mean values of products of rapidly varying quantities. These new terms are known as the Reynolds Stresses, and solution of the equations initially involves the construction of suitable models to represent these Reynolds Stresses. One approach is to treat the time averaged terms as additional viscous stresses produced by the turbulence in the flow. In the Boussinesq approximation the Reynolds Stresses are assumed to have a form identical to the viscous stresses in the momentum equation, apart from a multiplicative term known as the turbulent viscosity, μ_T.

Fluent provides several turbulence models based on the Boussinesq approach: the Spalart-Allmaras model [45], the k-ε model [24, 30,53], and the k-ω model [53]. As discussed in section 2 however, none of these models have proven to be particularly effective at capturing the time dependent features of the flow past a sphere at moderately large Reynolds numbers. This is in contrast to the findings of Iaccarino *et al.* [20], who carried out URANS (Unsteady Reynolds Averaged Navier Stokes) simulations of flow around square cylinders and a wall-mounted cube and found good agreement of the time-dependent features of the flow (such as the frequency of vortex shedding) with available experimental data. Constantinescu and Squires [7] however have noted that URANS simulations past spheres appear to be practically steady-state when compared with the results obtained from URANS simulations past cylinders, and they attribute these differences to the fact that the coherence of the wake structures in the flow past spheres is less significant as compared to the flow past cylinders.

Given the results of Drikakis [10] and Constantinescu and Squires [7] showing that URANS calculations are unable to capture the full time-dependent structure of flow past a sphere, and the results of Tomboulides *et al.* [51], Constantinescu and Squires [7] and Kim [25], which demonstrate superior predictive capabilities using both LES (Large Eddy Simulation) and DES (Detached Eddy Simulation) schemes, no attempts were made to simulate turbulent flow structures around a sphere using URANS calculations. All turbulent flow calculations reported here used the LES scheme, which is described in more detail in the next section.

4.2 Filtering

The alternative to Reynolds averaging is filtering. The idea behind this approach is to filter the time-dependent Navier-Stokes equation in either Fourier (wave-number) space or configuration (physical) space. This filtering process effectively filters out turbulent eddies whose scales are smaller than the filter width, which is usually taken to be the mesh size. A simulation using this approach is known as a Large Eddy Simulation (LES). As with Reynolds averaging however, the filtering process creates additional unknown terms which must be modelled in order to provide closure to the set of equations. These terms are the sub-grid scale stresses and Fluent 6.2 provides several models for these stresses. The simplest of these is the model originally proposed by Smagorinsky [44], in which the sub-grid scale stresses (SGS) are computed using an isotropic eddy viscosity approach which sets the SGS equal to the product of an eddy-viscosity and the resolved rate of strain tensor. The eddy viscosity is then calculated from an algebraic expression involving the product of a model constant C_S, the modulus of the rate of strain tensor, and an expression involving the filter width. The problem with this approach is that there is no single value of the constant C_S which is universally applicable to a wide range of flows. Another problem is that the model is not applicable to transitional flows because the basic expression always gives a finite value for the SGS viscosity even in laminar regions of the flow, as long as there is a velocity gradient. An additional problem is that an ad hoc damping is needed in the near-wall region.

Fluent 6.2 offers several LES models which overcome these failings of the original Smagorinsky model. The WALE model (Wall Adapting Local Eddy Viscosity) contains a near-wall modification in the expression for the SGS viscosity which adapts to the local near-wall flow structure and accounts for wall damping effects without using a damping function

explicitly. Fluent 6.2 also contains the Dynamic Smagorinsky Model (DSM) devised by Germano *et al*. [12] and Lilly [33]. In this procedure C_S is dynamically computed during the simulation using the information provided by the smaller scales of the resolved fields. C_S determined in this way varies with time and space and this allows the Smagorinsky model to cope with transitional flows and to include near-wall damping effects in a natural manner.

Another SGS LES model in Fluent 6.2 is the Localised Dynamic Kinetic Energy Model (LDKEM) of Kim and Menon [28,29]. In this model the SGS eddy viscosity is computed from an expression involving the filter width, the SGS turbulent kinetic energy, and a (dynamically computed) constant C_S. This model is more involved in that an additional transport equation needs to be solved for the SGS turbulent kinetic energy, but the LDKEM has several desirable attributes which the DSM lacks. In particular, using the SGS turbulent kinetic energy to parameterise the SGS stress renders the LDKEM better suited to non-equilibrium flows. A problem with any LES calculation is the treatment of wall boundaries. In Fluent 6.2, if the mesh is fine enough to resolve the laminar sublayer (as is the case in the simulations discussed in Section 6) the use of wall functions is avoided by calculating the wall shear stress from the laminar stress-strain relationship.

Another approach is known as Detached Eddy Simulation (DES). This was first proposed by Spalart [45, 46] in an attempt to combine the most favourable aspects of RANS and LES. DES reduces to a RANS calculation near solid boundaries and a LES calculation away from the wall. Fluent 6.2 offers a RANS / LES hybrid model based on the Spalart-Allmaras turbulence model near the wall and a one-equation SGS turbulence model away from the wall which reduces to an algebraic turbulent viscosity model for the SGS turbulence far from the wall.

5. Simulation Results for Laminar Flow

5.1 Steady axisymmetric regime: 20 < Re < 210

Section 2 describes the flow over a sphere as being both axisymmetric and steady up to a Reynolds number of approximately 210. To test the software in this range a run was first performed at Re = 100 on an axisymmetric mesh containing 198,694 quadrilateral cells. The sphere was located at the origin and had a diameter of 1.0 m. The flow was in the X direction with a velocity of 0.147 cm / s and the viscosity and density were those of ambient air, i.e. 1.7894×10^{-5} kg / (m-s) and 1.225 kg / m^3 respectively. The mesh extended from 10 m upstream of the sphere to 20 m downstream and the radial extent of the mesh was 12 m. The laminar calculation was run with the segregated solver in axisymmetric geometry using the cell based gradient option. The Pressure-Velocity coupling used the SIMPLE method and the momentum equations were solved using second-order upwind discretisation. The run had converged after approximately 1000 iterations and the calculated value of the drag coefficient was $C_d = 1.087$.

In order to check any dependence of this result on the resolution of the grid a region of the mesh between X = –4 m to X = 4 m and Y = 0 to Y = 4 m was refined using the Fluent grid adaption feature. The method works by isotropically subdividing each cell, so that a

quadrilateral cell is split into four equivalent quadrilateral cells. This increased the number of cells on the mesh from 198 694 cells to 240 470 cells. The value of the drag coefficient from this simulation, to four significant figures, was again $C_d = 1.087$.

To check any dependence of this result on the location of the boundaries a new mesh was constructed which extended from 15m in the upstream direction to 25 m in the downstream direction and out to 15 m in the radial direction. The grid spacing was kept to approximately 8 mm along the sphere surface and the height of the first cell was approximately 4 mm, with successive cell heights increasing with a ratio of 1.02. The total number of cells in the mesh was 277 344. The calculated value of the drag coefficient was $C_d = 1.086$. This value was also confirmed to be independent of grid resolution by again adapting the grid in the region between X = –4 m to X = 4 m and Y = 0 to Y = 4 m. The calculated value of the drag coefficient was again found to be $C_d = 1.086$.

The value for the drag coefficient calculated using Fluent on the smaller of the unrefined meshes ($C_d = 1.087$) compares favourably with the results found by many other authors. Tabata and Itakura [47] have performed a precise computation of the drag coefficient of a sphere in the range between Re = 10 and Re = 200 using two finite element schemes for axisymmetric flow problems. One is an extension of the standard mixed finite element method to axisymmetric problems while the other is an extension of the stabilised finite element method. The combination of these two methods results in a consistent flux method which allows them to obtain error estimates for the drag coefficient. Their method for Re = 100 gives $C_d = 1.0900 \pm 0.0003$. Clift, *et al.* [5] cite a value of $C_d = 1.087$, while Le Clair, *et al.* [31] calculated a value of $C_d = 1.096$ at this Reynolds number. Mittal [37] has used a Fourier-Chebyshev spectral collocation method for simulating flow past spheres and spheroids in the Reynolds number range between Re = 50 and Re = 500 and finds $C_d = 1.09$ at Re = 100.

In order to further validate the software in this Reynolds number range a series of computations was performed on the smaller, unrefined mesh, between Re = 20 and Re = 200. Figure 1 shows the calculated values of the drag coefficient in this range, as well as the experimental correlation of Clift, *et al.* [5] and Putnam [41], the calculated values of Tabata and Itakura [47] and Mittal [37] and the experimental results of Roos and Willmarth [42]. There is excellent agreement between the Fluent simulations and the experimental and simulation results of other authors.

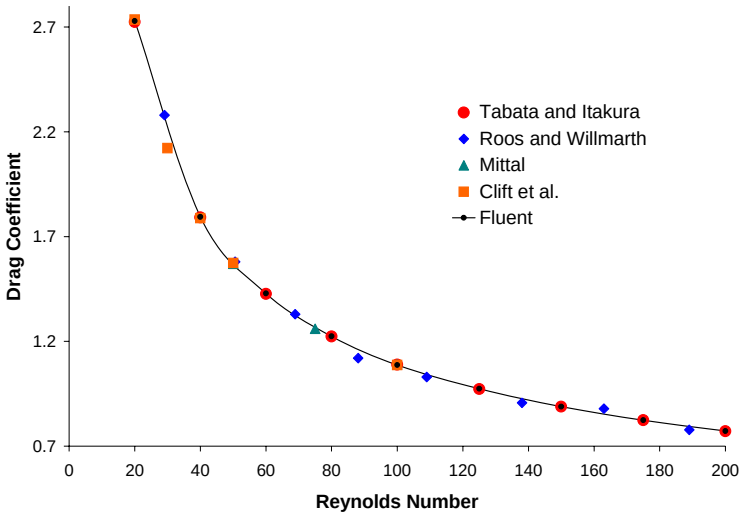

Figure 1: Comparison of computed drag coefficient with the experimental correlation of Clift, et al. [5], the calculated values of Tabata and Itakura [47] and Mittal [37], and the experimental results of Roos and Willmarth [42]

5.2 Unsteady planar-symmetric regime: Re = 300

Because of the loss of axial symmetry at higher Reynolds numbers a three-dimensional grid is needed for all simulation runs conducted above Re = 210. This was constructed by creating a sphere of 1 m diameter at the origin and then enclosing the sphere in a larger sized cube. A smaller cube was then inserted inside the sphere and then six hexagons were created by connecting the corner points of the inner cubes to the corner points of the outer cube. All redundant geometrical entities were then deleted and only the sphere faces retained. The sphere surface was then meshed with quadrilaterals having side lengths of approximately 5 mm and then hexagonal cells were created with the first cell height being approximately 15 mm and further cell heights having expansion ratios of approximately 1.08. The three-dimensional geometry was then meshed using the Gambit mapping option. The boundaries of the mesh extended from X = –8 m to X = 10 m, Y = –8 m to Y = 8 m and Z = –8 m to Z = 8 m. The total number of hexahedral cells was 965 120.

The three-dimensional grid was first tested by running a simulation at Re = 100. The calculated drag coefficient had a value of 1.0979 and the value of the lift coefficient was 1.4480×10^{-7}, indicating that the solution is effectively axisymmetric even though the calculation was carried out on a three-dimensional mesh. The grid was then refined using grid adaptation in the region X = –2 m to X = 2 m, Y = –2 m to Y = 2 m and Z = –2 m to Z = 2 m. The converged value of the drag coefficient was then $C_d = 1.0985$, i.e. approximately 0.05% higher. This indicates that the mesh has sufficient grid resolution near the surface of the sphere. The value 1.0985 is approximately 1% higher than the value of 1.087 calculated on the axisymmetric mesh though and indicates that there may still be some slight dependence of the value on the location of the boundaries.

A time-dependent run on the three-dimensional mesh was then performed at a Reynolds number of 300. The simulation was again run in laminar mode using the segregated solver, the SIMPLE Pressure-Velocity coupling, second-order upwind discretisation and the cell based gradient option. The run was started from the time-independent solution found at Re = 100 and the simulation was allowed to run without perturbation until numerical round-off errors resulted in the appearance of a regular periodic solution.

It was found that a considerable period of time was required to elapse before the motion settled into a regular periodic pattern. Figure 2 shows a plot of the drag coefficient as a function of time between t = 480 seconds and t = 560 seconds. The mean drag coefficient and its rms amplitude calculated from Figure 1 are 0.668 and 0.004 respectively. Johnson and Patel [23] obtained 0.656 and 0.004, Constantinescu, *et al*. [8] also obtained 0.656 and 0.003, while Tomboulides, *et al*. [50] calculated 0.671 and 0.003. Giacobello [13] calculated a mean drag coefficient of 0.658, while Kim, *et al*. [27] calculated a value of 0.657. The time step used for this run was 0.05 seconds. Reduction of this value to 0.025 seconds produced no change in the value of the mean drag coefficient.

It should be noted that Johnson and Patel and Constantinescu, *et al*. used a very similar meshing scheme and that both had an effective blockage ratio, defined as the sphere's frontal area divided by the computational grid's frontal area, of about 0.11%. The mesh for the three-dimensional calculations described here has a blockage ratio approximately three times this value, i.e. 0.31%. The simulation run on the three-dimensional mesh at Re = 100 resulted in a drag coefficient approximately 1% higher than the value calculated on the two-dimensional axisymmetric mesh (which had a blockage ratio of approximately 0.1%). If we assume that a similar reduction in the value of the drag coefficient would result from a Fluent run on a mesh having a blockage ratio of approximately 0.1% instead of 0.3% then the calculated value of 0.668 would reduce to 0.661, which is less than one percent different from the result obtained by Johnson and Patel and Constantinescu and Squires. The blockage ratio for the calculations of Tomboulides, *et al*. [50] was 1.23%, which may explain their higher value of $C_d = 0.671$.

The Strouhal number calculated from Figure 2 is 0.133. Johnson and Patel [23] obtained $S_t = 0.137$, Constantinescu *et al*. [8] found $S_t = 0.136$, while Tomboulides, *et al*. [50] obtained $S_t = 0.136$. Giacobello [13] calculated a value of 0.134 while Kim, *et al*. [27] also found a value of 0.134. The value measured by Sakomoto and Haniu [43] at Re = 300 is in the range of 0.15 - 0.16. The time step used by Johnson and Patel [23] was 0.05 seconds while Tomboulides, *et al*. [50] used a much smaller time step of 0.005 seconds. Whilst reducing the time step in our calculation from 0.05 seconds to 0.025 seconds produced no change in the mean value of the drag coefficient, it did result in a slight increase in the Strouhal number, from 0.133 to 0.136. This compares well with the values calculated by other authors and the experimental results.

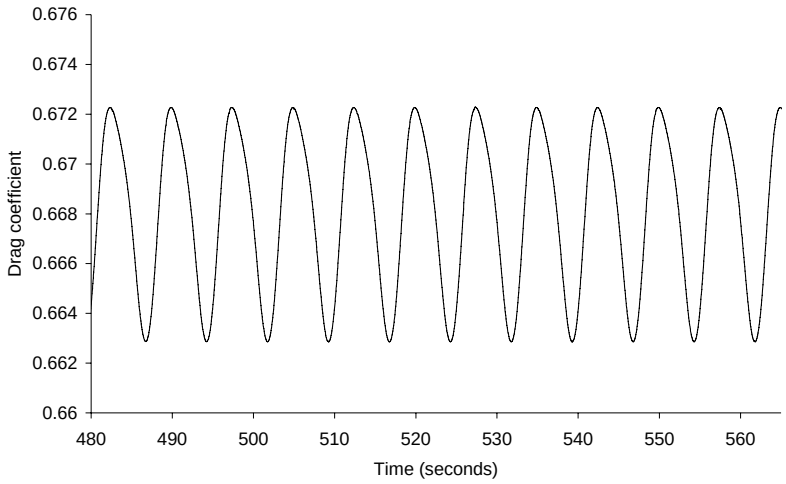

Figure 2: Drag coefficient versus time at Re =300

The periodicity of the flow at Re = 300 is due to the regular shedding of vorticity. As described by Magarvey and Bishop [34], the wake consists of a series of interconnected vortex loops above Re = 290, while Sakamoto and Haniu [43] show that hairpin shaped vortices begin to shed periodically at Re = 300. To observe the shedding of vorticity in the simulation results presented here we have used the Q method of vortex identification. This is one of several methods which have been proposed and discussed in the literature recently. Jeong and Hussain [22] conducted an extensive series of tests on several vortex identification methods to determine the most appropriate method of identifying a vortex in a turbulent flow. They considered the following methods:

1. Local pressure minimum
2. Closed or spiralling streamlines and pathlines
3. Iso-contours of vorticity magnitude (i.e. $|\boldsymbol{\omega}|$, where $\boldsymbol{\omega}$ is the vorticity, $\boldsymbol{\omega} = \nabla \times \mathbf{u}$, and $\mathbf{u}$ is the flow velocity)
4. The occurrence of complex eigenvalues of the velocity gradient tensor $\nabla\mathbf{u}$, which is equivalent to the statement that the discriminant of the characteristic equation for the eigenvalues is positive
5. The Q method, where Q is the positive second invariant of the deformation tensor. i.e. $Q = (\Omega_{ij} \Omega_{ij} - S_{ij} S_{ij}) / 2$, where $\Omega_{ij} = (\partial u_i / \partial x_j - \partial u_j / \partial x_i) / 2$ and $S_{ij} = (\partial u_i / \partial x_j + \partial u_j / \partial x_i) / 2$. A vortex exists when $Q > 0$
6. The λ_2 method, where a vortex is defined as a connected region of space with two negative eigenvalues of the tensor $\mathbf{S}^2 + \boldsymbol{\Omega}^2$ (where $\mathbf{S}$ and $\boldsymbol{\Omega}$ are defined above). Since $\mathbf{S}^2 + \boldsymbol{\Omega}^2$ is symmetric and has three real eigenvalues λ_1, λ_2 and λ_3 this definition is equivalent to the statement that $\lambda_2 < 0$ if the eigenvalues are ordered such that $\lambda_1 \geq \lambda_2 \geq \lambda_3$

Their conclusion was that only the λ_2 method represented the topology and geometry of vortex cores correctly for the large variety of flows considered in their analyses, although they did also state that, in most cases, the Q and λ_2 methods did result in similar vortex cores. Lesieur, *et al*. [32] have also done a comparison of vortex identification methods including local pressure minimum, iso-contours of vorticity magnitude, positive Q and negative λ_2 and their results also show great similarities between vortex cores identified using the positive Q and negative λ_2 methods. Giacobello [13] has recently simulated flow around a sphere at Re = 300 using a spherical polar coordinate system and a Fourier-Chebyshev collocated method as part of a broader study looking at the wake structure of transversely rotating spheres. He elucidated the vortex structure in the wake using iso-surfaces of streamwise vorticity, iso-surfaces of vorticity magnitude, the Q method, and the λ_2 method, amongst others. He also concluded that the λ_2 method provided the best representation of the vortex structure in the flow, although he also noted that the Q method and the λ_2 criteria produced very similar vortex structures. Given that the two methods produce very similar structures for the flow around a sphere, and that the Q method is far easier to implement in Fluent, we have decided to use the Q method for the simulation results described here.

Figure 3 shows contours of velocity magnitude plotted on iso-contours of Q at the time t = 675.35 seconds. Giacobello [13] noted that an important property of a vortex identification criteria (which is amply satisfied by the λ_2 method) is that it should be insensitive to the threshold value used for the visualisation. We have also found this to be true in the case of the Q method as quite large changes in the iso value lead to identical vortex structures. Figure 3 clearly shows the shear layer separating from the sphere surface and the tubular vortical structure in the far wake.

Figure 4 shows a different perspective of the same plot. This clearly shows the planar symmetry which still persists in the flow at this Reynolds number, as noted by Sakamoto and Haniu [43] experimentally, and as demonstrated by Mittal [36] in his numerical simulations.

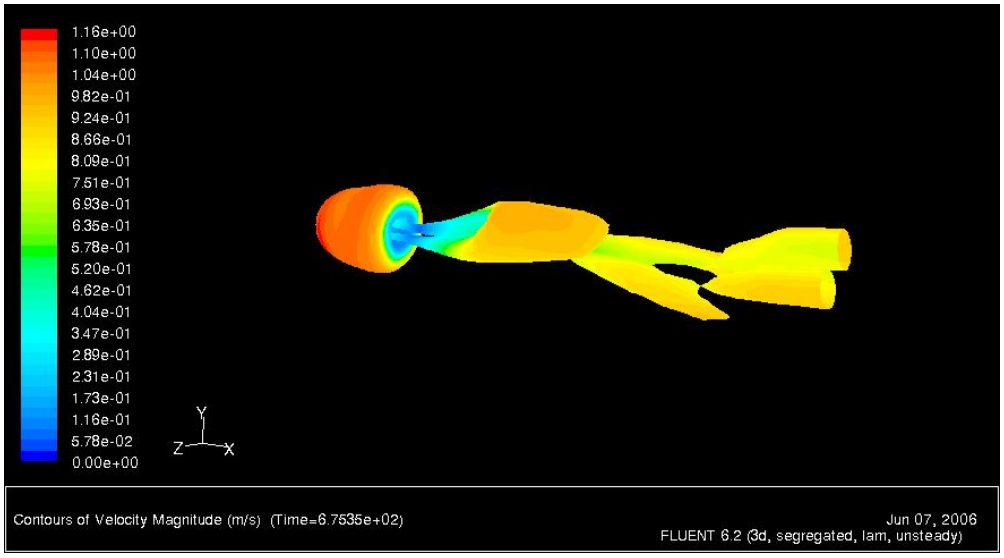

Figure 3: Contours of velocity magnitude at Re = 300 plotted on iso-contours of the second invariant of the deformation tensor

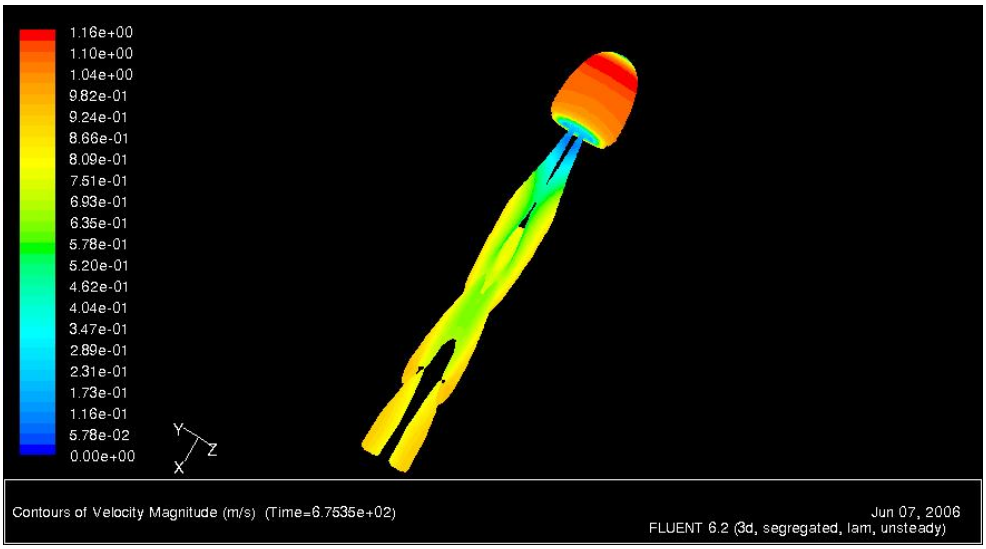

Figure 4: Contours of velocity magnitude at Re = 300 plotted on iso-contours of the second invariant of the deformation tensor

6. Simulation Results for Turbulent Flow

As discussed in Section 2.5, URANS simulations are unable to capture the fine scale time dependent features of the turbulent flow around a sphere such as the high frequency (Kelvin-Helmholtz instability) mode found in the experimental results of Sakomoto and Haniu [43], or the presence of the higher frequency band seen in the simulations by Constantinescu and Squires [7]. Fortunately Fluent 6.2 contains both LES and DES turbulence models as well as considerably enhanced discretisation schemes which are suited to the effective utilisation of these advanced models.

As described in Section 4.2, Fluent 6.2 offers an LES model with the original Smagorinsky expression for the sub-grid scale stresses or three advanced LES models; WALE, LDKEM, or the Dynamic Smagorinsky model. The DES model in Fluent 6.2 uses a Spalart-Allmaras turbulence model near the wall and a one-equation SGS turbulence model away from the wall.

Kim [25] has used the LES model on unstructured meshes to simulate flow around a sphere for Reynolds numbers of 1.0×10^4 and 1.14×10^6 using both the dynamic Smagorinsky model and the LDKEM, but found that there was little difference in the results predicted by the two models. Constantinescu, *et al*. [8] have also simulated the flow over a sphere at a Reynolds number of 1.0×10^4 using both LES and DES models and found that both methods gave essentially the same results. In this section we use the Fluent LES model with the Dynamic Smagorinsky SGS model to simulate flows at $Re = 1.0 \times 10^4$ and $Re = 1.0 \times 10^6$. Because the boundary layer is considerably thinner at these higher Reynolds numbers we increased the grid resolution in this region by constructing a new grid containing 2.6 million hexahedral cells. The method of construction and outer limits of the mesh remain the same as those of the earlier mesh but the cell density has been increased over the surface of the grid and in the near-wake region.

6.1 Reynolds number = 10^4

The time-dependent run was started from an initial mean flow calculated from a steady-state RANS calculation using the k-ε model. The inflow velocity was 0.146 m / s and the time step was 0.137 seconds. This corresponds to about 250 timesteps per oscillation based on a known experimental Strouhal number of approximately 0.2 at this Reynolds number. The flow structure at $Re = 1.0 \times 10^4$ is remarkably different to that at $Re = 300$ as can be seen from Figure 5, which shows the vorticity structure of the flow using the Q method described in the previous section.

The additional complexity in the flow is also evident in the plot of drag coefficient as a function of time, shown in Figure 6. In addition to the main frequency due to the vortex shedding, which occurs at a Strouhal number of 0.191 in Figure 6, the time history also shows an additional high frequency component in the range 1.65 to 1.82 which is associated with the Kelvin-Helmholtz instability in the detached shear layers, as noted by Constantinescu and Squires [7]. These results agree well with those of the LES simulations of Constantinescu, *et al.* [8], who found a value of $S_t = 0.195$ for the fundamental shedding frequency, as well as a

second high frequency band occurring between $S_t = 1.30$ and $S_t = 1.85$. Kim [25] found $S_t = 0.182$ using an unstructured hybrid mesh of 2.46 million cells using LES with a Dynamic Smagorinsky SGS model. The mean drag coefficient calculated over the length of the run was 0.387. Constantinescu, *et al.* [8] obtained 0.393 ± 0.014 while Kim [25] calculated a value of 0.438. The experimental value (from Achenbach [2]) is $C_d = 0.40 \pm 0.01$.

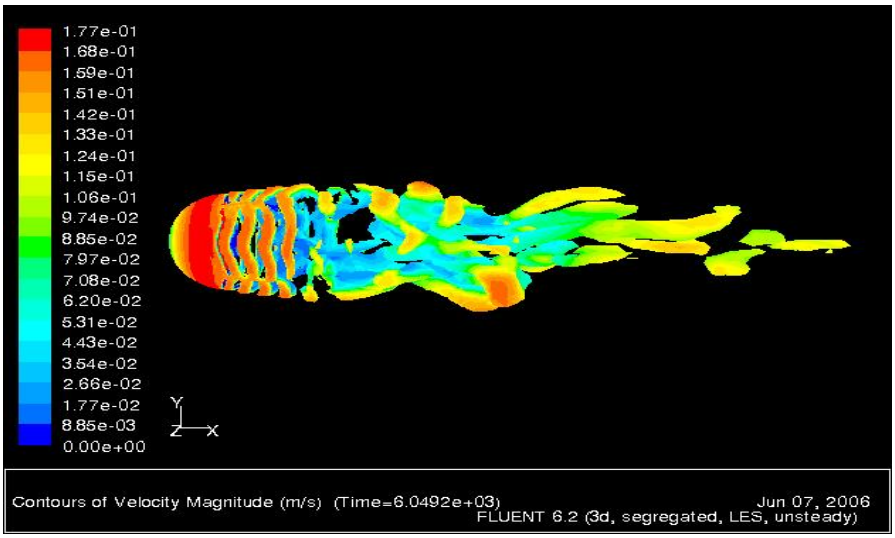

Figure 5: Contours of velocity magnitude at $Re = 1.0 \times 10^4$ plotted on iso-contours of the second invariant of the deformation tensor

Figure 7 shows the Y component of the lateral force coefficient as a function of time. This displays a fundamentally different time structure to that shown by the drag coefficient. The Strouhal number estimated from Figure 7 lies in the range $S_t = 0.151 - 0.158$ and there is no evidence of a high-frequency component associated with the shear-layer instability. Constantinescu and Squires [7] found two dominant frequencies in the ranges $S_t = 0.06 - 0.08$ and $S_t = 0.15 - 0.16$ and also noted the absence of a high-frequency component associated with the shear layer instability. They stated that this was explained by the fact that the vortex tubes shed at the higher Strouhal number are positioned approximately in planes perpendicular to the free stream direction and the resulting force on the sphere is therefore oriented parallel to this direction. They also noted that the difference in frequency between the lateral force oscillations and the oscillations in the drag coefficient also occur for cylinders.

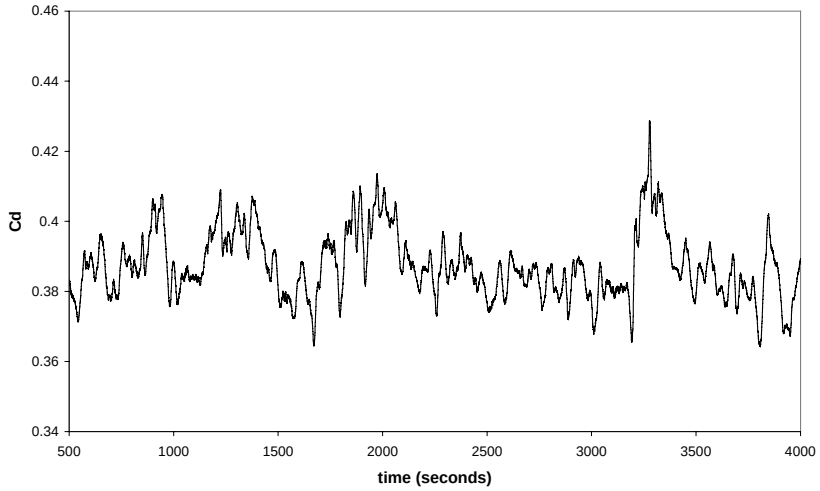

Figure 6: Drag coefficient versus time at Re = 1.0 $\times 10^4$

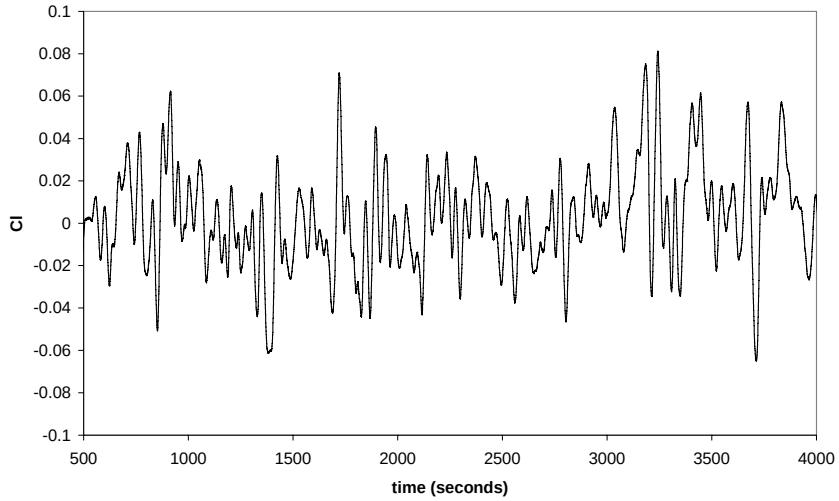

Figure 7: Y component of lateral force coefficient versus time at Re = 1.0 $\times 10^4$

Figure 8 shows streamlines over the surface of the sphere from two different viewpoints. These clearly show the location of boundary layer separation as well as the extent of variation in the azimuthal direction. From these figures we estimate that separation occurs at a polar angle of 88.0° ±1°. This is slightly larger than the value of 85.0° ± 1° found by Constantinescu, *et al.* [8] in their LES simulations although it is closer to the value found by Kim [25], who found a separation angle in the range 86° ~ 87°. We note that the y^+ value over the surface of the sphere near the separation region is in the range $y^+ = 0.2$ to $y^+ = 0.7$.

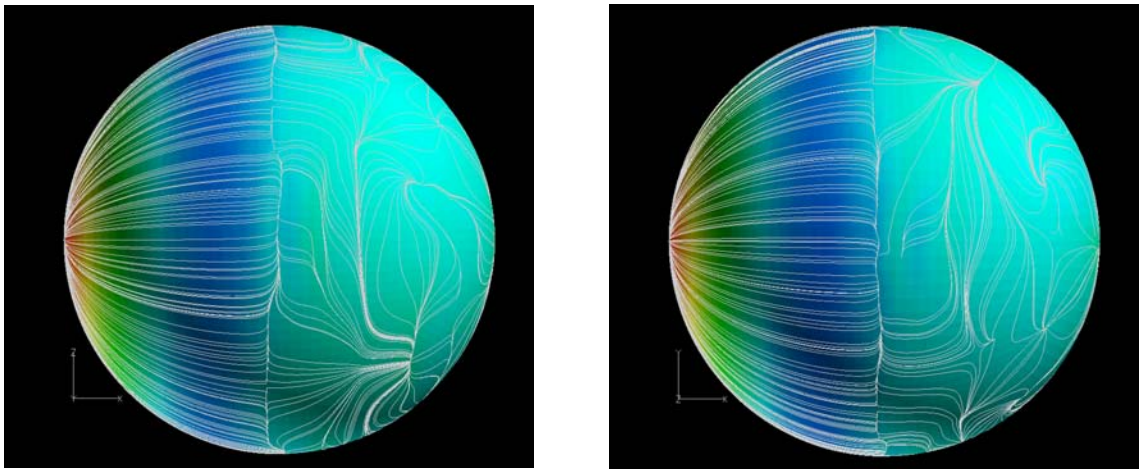

a b

Figure 8: a) Surface streamlines viewed along the Y axis at Re = 10^4. b) Surface streamlines viewed along the Z axis at Re = 10^4.

6.2 Reynolds number = 10^6

To perform simulations at a Reynolds number of 10^6 the grid used for the previous simulation at Re = 10^4 was further refined in a region close to the sphere surface to ensure adequate resolution of the thinner boundary layer at this higher Reynolds number. The mesh contained 3.3 million hexahedral cells and resulted in a wall y^+ value which varied between 0.3 and 0.9 over the surface of the sphere during the course of the simulation.

The simulation was again started from an initial mean flow calculated from a steady-state RANS calculation using the k-ε model. The inflow velocity was 14.6 m/s and the time step used was 0.001 seconds. At this Reynolds number the flow is well above the "drag crisis" which occurs at approximately Re = 3.8×10^5 and we would therefore expect the sphere to exhibit a much lower drag coefficient and that separation would occur much closer to the downstream stagnation point. This is qualitatively evident from Figure 9, which shows the vorticity structure in the flow.

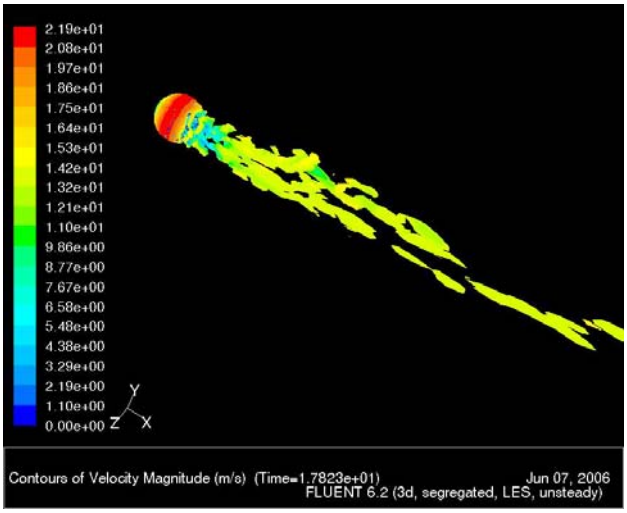

a

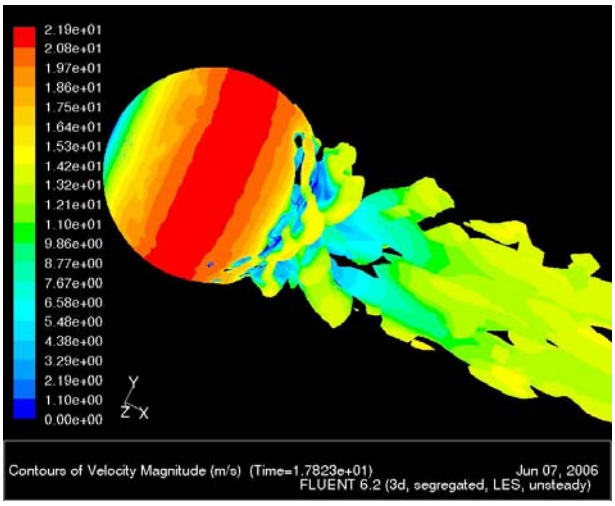

b

Figure 9: a) Contours of velocity magnitude at Re = 1.0 × 10^6 plotted on iso-contours of the second invariant of the deformation tensor. b) Contours of velocity magnitude at Re = 1.0 × 10^6 plotted on iso-contours of the second invariant of the deformation tensor. Enhanced view of Figure 9a.

The dramatic change in the flow structure is easily seen by comparing Figure 5 and Figure 9. The close-up view in Figure 9b in particular shows that the wake at the higher Reynolds number is much narrower, as expected, due to the delayed onset of flow separation in the now turbulent boundary layer.

Figure 10 shows the drag coefficient as a function of time. The mean value is 0.104. Kim [25] found C_d = 0.139 using the dynamic Smagorinsky model and C_d = 0.142 using the LDKEM at Re = 1.14 × 10^6. Constantinescu and Squires [7] found C_d = 0.080 at Re = 1.14 × 10^6 in their DES simulation, and also found that C_d = 0.102 if they forced the boundary layer to remain fully turbulent before separation. Wang and Kannan [52] used an overset adaptive cartesion / prism

grid method with 2.1 million cells and a Spalart-Almaras turbulence model and found $C_d = 0.09$. Jindal, *et al*. [21] also conducted an LES simulation on a sphere at $Re = 1.14 \times 10^6$ on an unstructured tetrahedral mesh with 2.5 million cells using the dynamic Smagorinsky model and the instantaneous logarithmic law of the wall to model the wall shear stress. They found $C_d = 0.141$. The experimental value from Achenbach [2] is $C_d = 0.12$.

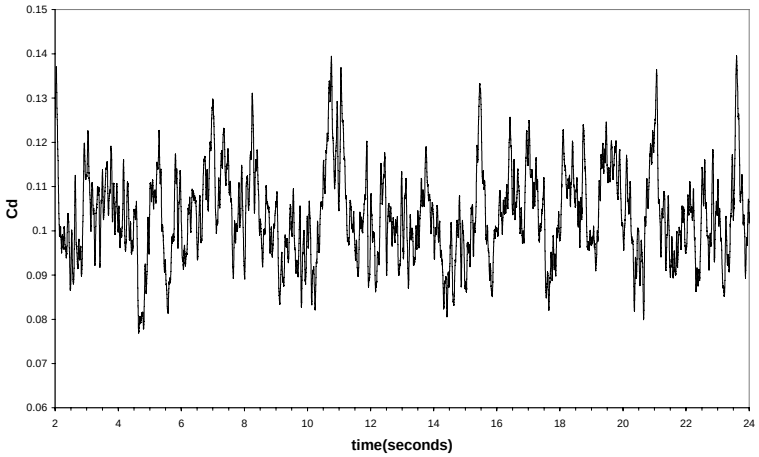

Figure 10: Drag coefficient versus time at Re = 1.0 × 10⁶

Figure 11 shows streamlines over the surface of the sphere. Although there is obviously more variation in the location of the separation line in the azimuthal direction than occurred for the case of $Re = 1.0 \times 10^4$ it is still possible to estimate an average separation angle of $121° \pm 2°$. This compares well with the results of Constantinescu and Squires [7], who found $\theta_s = 120° \pm 2°$ at $Re = 1.14 \times 10^6$, and also with the experimental value from Achenbach [2] of $\theta_s = 120°$. Wang and Kannan [52] found $\theta_s = 115°$, Jindal, *et al.* [21] found $\theta_s \sim 120°$, while Kim [25] found $\theta_s \sim 100°$. As noted by Kim [25], the discrepancy in this case was undoubtedly due to insufficient resolution in the boundary layer.

Figure 12 shows the frequency spectrum of the time history of the drag coefficient. Peak power is observed at $S_t = 0.048$ and this agrees well with the result found by Jindal, *et al.* [21] who found a peak at a Strouhal number of $S_t \sim 0.05$. Constantinescu and Squires [7] however found a peak in the frequency spectrum at $S_t = 1.30$ for $Re = 1.14 \times 10^6$.

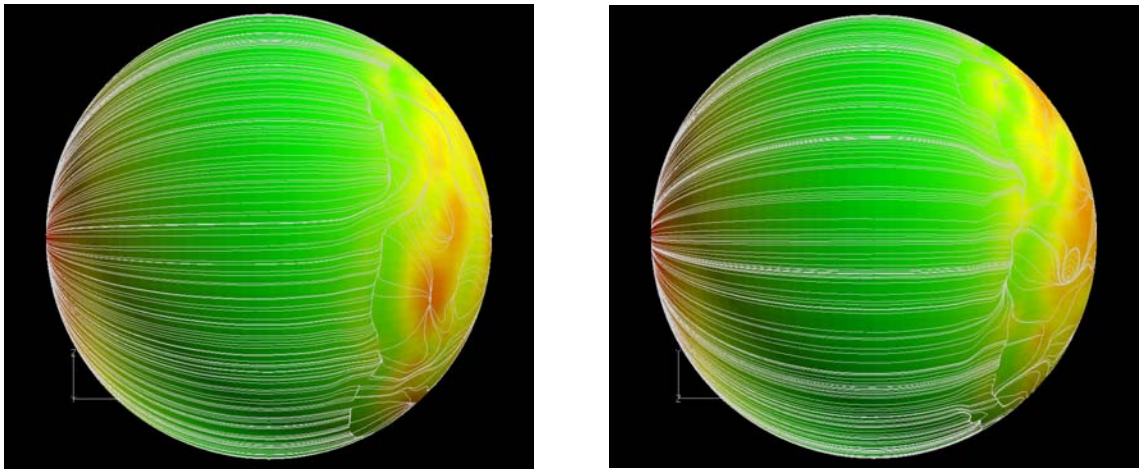

a b

Figure 11: a) Surface streamlines viewed along the Y axis at Re = 10^6. b) Surface streamlines viewed along the Z axis at Re = 10^6.

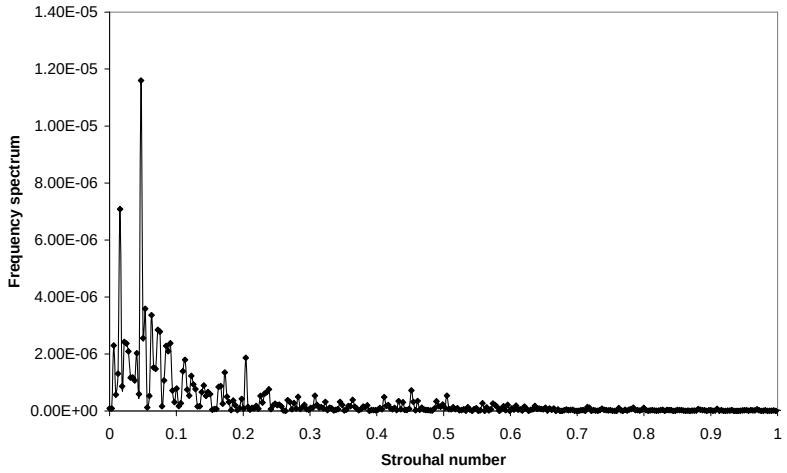

Figure 12: Plot of frequency spectrum as a function of Strouhal number calculated by taking the FFT of C_d versus time at Re = 1.0 $\times 10^6$

7. Discussion and Conclusion

In this section we briefly review the simulation results for the various flow regimes. A summary of the data for the computed mean drag coefficient (C_d), Strouhal number (S_t) and mean separation angle (θ_s) is given in Table 2. Between Re = 20 and Re =200, where the flow is steady-state, axisymmetric and laminar the simulated value for the drag coefficient was in excellent agreement with results found both experimentally and computationally by other authors. In particular, at Re = 100, the drag coefficient was calculated to be $C_d = 1.086$, which compares favourably with the experimentally calibrated value of $C_d = 1.087$ found by Clift, *et al.* [5] and the precise computation of Tabata and Itakura [47], which found $C_d = 1.0900 \pm 0.0003$.

At Re = 300 the flow becomes unsteady and transitions into periodic time-dependent behaviour due to the regular shedding of hairpin shaped vortices. The mean drag coefficient, after correction for blockage ratio effects, was calculated to have the value 0.661. This compares very favourably with the value of $C_d = 0.656$ obtained by both Johnson and Patel [23] and Constantinescu, *et al.* [8]. Giacobello [13] calculated $C_d = 0.658$, while Kim, *et al.* [27] calculated a value of 0.657. The corresponding Strouhal number calculated from this simulation was $S_t = 0.133$, which also compares favourably with the value found by Giacobello [13] and Kim, *et al.* [27], who both calculated $S_t = 0.134$, while Johnson and Patel [23] obtained $S_t = 0.137$ and Constantinescu, *et al.* [8] found $S_t = 0.136$.

At Re = 10^4 the flow in the wake becomes turbulent while the flow in the boundary layer remains laminar. An LES simulation using the Dynamic Smagorinsky sub-grid scale model with a fine mesh to resolve the laminar sublayer was used for this Reynolds number. The simulated results were in good agreement with both experimental results and other numerical simulations. The time-dependent behaviour becomes considerably more complex and in addition to the main frequency due to the vortex shedding, which now occurs at a Strouhal number of 0.191, the time history also shows an additional high frequency component in the range 1.65 to 1.82. These results agree well with those of the LES simulations of Constantinescu, *et al.* [8], who found a value of $S_t = 0.195$ for the fundamental shedding frequency, as well as a second high frequency band occurring between $S_t = 1.30$ and $S_t = 1.85$. The mean drag coefficient was 0.387, which agrees with the value obtained by Constantinescu, *et al.* [8] of 0.393 ± 0.014 and is very close to the experimental value of $C_d = 0.40 \pm 0.01$ (Achenbach [2]).Streamline plots over the surface of the sphere showed that boundary layer separation occurs at a polar angle of $88.0° \pm 1°$, which is slightly larger than the value of $85.0° \pm 1°$ found by Constantinescu, *et al.* [8] but is closer to the value calculated by Kim [25], who found θ_s to be approximately $86° \sim 87°$.

At a Reynolds number of approximately Re = 3.8×10^5 the boundary layer switches from being predominantly laminar to predominantly turbulent, hence the separation point moves further downstream, the wake narrows, and the drag coefficient drops considerably, from around $C_d = 0.40$ at Re = 1.0×10^4 to approximately $C_d = 0.08$. A further increase in Reynolds number then leads to a slow increase in the drag coefficient again until $C_d \sim 0.20$ at Re ~ 4.0×10^6. The Fluent LES simulation at Re = 1.0×10^6 adequately captured this behaviour. The vorticity

structure of the flow showed that the wake was much narrower at the higher Reynolds number. The average separation angle was found to be 121° ± 2°, which agrees with the results of Constantinescu and Squires [7], who found $\theta_s = 120° \pm 2°$ at $Re = 1.14 \times 10^6$, and also with the experimental value from Achenbach [2] of $\theta_s = 120°$.

Table 2: Summary of simulation results as a function of Reynolds number

Re	**C_d (Fluent)**	**C_d (calc/expt)**	**S_t (Fluent)**	**S_t (calc/expt)**	**θ_s (Fluent)**	**θ_s (calc/expt)**
100	1.087	1.087 [5] 1.0900 [47] 1.09 [37] 1.096 [31]	Not applicable	Not applicable	Not applicable	Not applicable
300	0.661	0.656 [23] 0.656 [8] 0.657 [27] 0.658 [13] 0.671 [50] 0.671 [49]	0.133	0.134 [13] 0.134 [27] 0.136 [8] 0.136 [50] 0.137 [23]	Not applicable	Not applicable
1.0×10^4	0.387	0.393 [8] 0.438 [25] 0.40±0.01 [2]	0.191 (S_t1) 1.65-1.82 (S_t2)	0.195 [8] S_t1 0.181 [25] S_t1 1.30-1.85[8]	88.0° ±1°	85.0° ±1° [8] 86.5°±1° [25]
1.0×10^6	0.104	0.080 [7] 0.09 [52] 0.12 [2] 0.139 [24] 0.141 [21] 0.142 [24]	0.048	0.05 [21] 1.30 [7]	121.0° ±2°	100° [25] 115° [52] 120.0° ±2° [7] 120° [2] 120° [21]

The simulation results described in this report have illustrated the capability of Fluent version 6.2 to accurately reproduce typical flow structures observed on this generic bluff body flow for both time independent / time-dependent and laminar / turbulent flow regimes.

8. Acknowledgements

The authors would like to thank Hawk Lee, David Graham and Ben Simpson in the Melbourne office of LEAP Australia for considerable technical help with several software problems during the course of this work.

9. References

1. Achenbach, E., "Experiments on the flow past spheres at very high Reynolds numbers", *J. Fluid Mech.*, **54**, pp. 565-575, 1972.
2. Achenbach, E., "Vortex shedding from spheres", *J. Fluid Mech.*, **62**, pp. 209-221, 1974.
3. CFX– Commercially available CFD software package based on the Finite Volume method. A product of AEA Technology Engineering Software, Didcot, Oxfordshire, UK. Distributed in Australia by ATD International Pty. Ltd., Hawthorn, Vic.

4. Chomaz, J.M., Bonneton, P. and Hopfinger, E.J., "The structure of the near wake of a sphere moving horizontally in a stratified fluid", *J. Fluid Mech.*, **254**, 1-21, 1993.

5. Clift, R., Grace, J.R. and Weber, M.E., "Bubbles, Drops and Particles", *Academic Pres*s, New York, 1978.

6. Constantinescu, G.S. and Squires, K.D., "Role of the turbulence model in prediction of flow over a sphere", *Proceedings of FEDSM'00 ASME Fluids Engineering Summer Meeting*, Boston, USA, pp. 69-75, 2000.

7. Constantinescu, G.S. and Squires, K.D., "Numerical investigations of flow over a sphere in the subcritical and supercritical regimes", *Phys. Fluids*, **16**(5), 1449-1466, 2004.

8. Constantinescu, G.S., Chapelet, M.C. and Squires, K.D., "Prediction of Turbulent Flow over a Sphere", *AIAA Journal*, **41**, 1733-1742 (2003).

9. Dallmann, U, Gebing, H. and Vollmer, H., "Unsteady Three-Dimensional Separated Flows Around a Sphere – Analysis of Vortex Chain Formation", in *Bluff-body wakes, dynamics and instabilities*, Eckelmann, H., Springer-Verlag (1993).

10. Drikakis, D., "Development and implementation of parallel high resolution schemes in 3D flows over bluff bodies", *Parallel Computational Fluid Dynamics: Implementations and Results Using Parallel Computers*, Elsevier Science, 191-198, 1995.

11. Fluent – Commercially available CFD software package based on the Finite Volume method. A product of Fluent Inc., Centerra Resource Park, 10 Cavendish Court, Lebanon, NH, USA. Distributed in Australia by LEAP Australia Pty. Ltd.

12. Germano, M., Piompelli, P.M. and Cabot, W.H., "Dynamic Subgrid Scale Eddy Viscosity Model", *Physics of Fluids A*, **3**, 1760-1765, 1991.

13. Giacobello, M., "Wake structure of a transversely rotating sphere at moderate Reynolds numbers", Ph.D. thesis, The University of Melbourne, Department of Mechanical Engineering, September 2005.

14. Gushchin, V.A., Kostomorov, A.V., Matyushin, P.V. and Pavlyukova, E.R., "Direct Numerical Simulation of the Transitional Separated Fluid Flows around a Sphere", Proceedings of the 7th Russian-Japanese CFD Workshop at Moscow State University, July 31st – August 4th, 2000, *Computational Fluid Dynamics Journal*, **10**, no. 3, pp. 344-349, 2001.

15. Huyer, S.A., Drack, L. and Jones, D.A., "The Vortel Computational Fluid Dynamics Code", *Draft DSTO Technical Report.*

16. Huyer, S.A. and Grant, J.R., "Computation of Unsteady Bow Thruster Hydrodynamics using a Lagrangian Vorticity Method", *3rd ASME/JSME Joint Fluids Engineering Conference*, San Francisco, CA, July, 1999.

17. Huyer, S.A. and Grant, J.R., "Computation of Two-Body Hydrodynamics Using a Lagrangian Vorticity Method", *International UUV Symposium, Newport, RI*, April, 2000.

18. Huyer, S.A. and Grant, J.R., "Simulation of UUV Recovery Hydrodynamics", *23rd Symposium on Naval Hydrodynamics*, September, 2000.

19. Huyer, S.A., Grant, J.R. and Uhlman, J.S., "Computation of Unsteady Separated Flow Fields Past an Oscillating Airfoil Using Discrete Vortex Elements", *AIAA 25th Fluid Dynamics Conference*, paper no. 94-2257, Colorado Springs, CO, June 1994.

20. Iaccarino, G., Ooi, A., Durbin, P.A. and Behnia, M., "Reynolds averaged simulation of unsteady separated flow", *Int. Journal of Heat and Fluid Flow*, **24**, 147-156, 2003.

21. Jindal, S., Long, L.N., Plassmann, P.E. and Sezer-Uzol, N., "Large Eddy Simulations around a sphere using unstructured grids", 24th AIAA Fluid Dynamics Conference and Exhibit, 28th Hune - 1st July, 2004, paper number AIAA 2004-2228.

22. Jeong, J and Hussain, F., "On the identification of a vortex", *J. Fluid. Mech.*, **285**, 69-94 (1995).

23. Johnson, T.A. and Patel, V.C., "Flow past a sphere up to a Reynolds number of 300", *J. Fluid Mech.* **378**, pp. 19-70, 1999.

24. Jones, W.P. and Launder, B.E. "The prediction of laminarisation with a two-equation model of turbulence", *Int. J. Heat Mass Transfer*, **15**, 301-314 (1972).

25. Kim, S.E., "Large Eddy Simulation Using Unstructured Meshes and Dynamic Subgrid-Scale Turbulence Models", *34th AIAA Fluid Dynamics Conference and Exhibit*, Portland, Oregon, *AIAA paper number 2004-2548*, 2004.

26. Kim, H.J. and Durbin, P.A., "Observations of the frequencies in a sphere wake and of drag increase by acoustic excitation", *Phys. Fluids*, **31** (11) 3260-3265, 1988.

27. Kim, J., Kim, D. and Choi, H., "An Immersed-Boundary Finite-Volume Method for Simulations of Flow in Complex Geometries", *Journal of Computational Physics*, **171**, 132 – 150 (2001).

28. Kim, W.W. and Menon, S., "A New Dynamic One-Equation Sub-Grid Scale Model for Large Eddy Simulations", *AIAA paper 95-0356*, 1995.

29. Kim, W.W. and Menon, S., "Application of the Localised Dynamic Subgrid-Scale Model to Turbulent Wall-Bounded Flows", *AIAA paper 97-0210*, 1997.

30. Launder, B.E. and Sharma, B.I. "Application of the energy-dissipation model of turbulence to the calculation of flow near a spinning disc", *Lett. Heat Mass Transf.*, **1**, 131-138 (1974)

31. Le Clair, B.P., Hamielec, A.E. and Pruppacher, H.R., "A numerical study of the darg on a sphere at low and intermediate Reynolds numbers", *J. Atmos. Sci.*, **27**, 308-315, 1970.

32. Lesieur, M., Métais, O. and Comte, P., "Large-Eddy Simulations of Turbulence", Cambridge University Press, 2005.

33. Lilly, D.K., "A Proposed Modification of the Germano Subgrid Scale Closure Model", *Physics of Fluids A*, **4**, 633-635, 1992.

34. Margavey, R.H. and Bishop, R.L., "Transition ranges for three-dimensional wakes", *Can. J. Phys.*, **39**, 1418-1422, 1961.

35. Marshall, J.S., Grant, J.R., Gossler, A.A. and Huyer, S.A., "Vorticity Transport on a Lagrangian Tetrahedral Mesh", *Journal of Computational Physics*, **161**, 85-113, 2000.

36. Mittal, R. "Planar Symmetry in the Unsteady Wake of a Sphere", *AIAA Journal*, **37**, 388-390, (1999).

37. Mittal, R. "A Fourier-Chebyshev Spectral Collocation Method for Simulating Flow past Sphere and Spheroids", Int. J. Numer. Meth. Fluids **30**, pp. 921-937, 1999.

38. Nakamura, I., "Steady wake behind a sphere", *Phys. Fluids*, **19**(1), pp. 5-8, 1976.

39. Natarajan, R. and Acrivos, A., "The instability of the steady flow past spheres and disks", *J. Fluid Mech.* **254**, 323-344, 1993.

40. Ploumhans, P., Winckelmans, G.S., Salmon, J.K., Leonard, A. and Warren, M.S. "Vortex Methods for Direct Numerical Simulation of Three-Dimensional Bluff Body Flows: Application to the Sphere at Re = 300, 500 and 1000", *J. Computational Physics*, **178**, 427-463, 2002.

41. Putnam, A., "Integrable Form of Droplet Drag Coefficient", *American Rocket Society Journal*, **31**(10), 1467-1468, 1961.

42. Roos, F.W. and Willmarth, W.W., "Some Experimental Results on Sphere and Disk Drag", *AIAA Journal*, **9**(2), 285-291, 1971

43. Sakamoto, H. and Haniu, H., "A study of vortex shedding from spheres in uniform flow", J. Fluids Eng., **112**, 386-393, 1990.

44. Smagorinsky, J., "General Circulation Experiments with the Primitive Equations, part 1: The Basic Experiment", *Monthly Weather Review*, **91**, 99-165, 1963.

45. Spalart, R.P. and Allmaras, S.R., "A one-equation turbulence model for aerodynamic flows", *La Recherche Aérospatiale*, **1**, 5-21 (1994).

46. Spalart, P.R., Jou, W.H., Strelets, M. and Allmaras, S.R., "Comments on the feasibility of LES for wings, and on a hybrid RANS/LES approach", *First AFOSR International Conference on DNS/LES*, Rouston, Louisiana, 1997.

47. Tabata, M. and Itakura, K., "A precise computation of drag coefficients of a sphere", Int. J. Comput. Fluid Dynam. **9**, 303, 1998.

48. Taneda, S., "Experimental Investigation of the Wake behind a Sphere at Low Reynolds Numbers", *J. Phys. Soc. Japan*, **11** (10), pp. 1104-1108, 1956.

49. Taneda, S., "Visual observations of the flow past a sphere at Reynolds numbers between 10^4 and 10^6", *J. Fluid Mech.*, **85**, 187-192, 1978.

50. Tomboulides, A.G., Orszag, S.A. and Karniadakis, G.E., "Direct and Large eddy simulations of axisymmetric wakes", *AIAA paper number 93-0546*, 1993.

51. Tomboulides, A.G. and Orszag, S.A. "Numerical investigation of transitional and weak turbulent flow past a sphere", *J. Fluid Mech.*, **416**, pp. 45-73, 2000.

52. Wang, Z.J. and Kannan, R., An Overset Adaptive Cartesian/Prism Grid Method for Moving Boundary Flow Problems", 43rd AIAA Conference, January 2005, paper number AIAA-2005-0322.

53. Wilcox, D.C., "Turbulence Modelling for CFD", 2nd edition, DCW Industries, Inc. (1998).

54. Wu, J.S. and Faeth, G.M., "Sphere wakes in still surroundings at intermediate Reynolds numbers", *AIAA J.*, **31**, 1448-1455, 1993.

DEFENCE SCIENCE AND TECHNOLOGY ORGANISATION
DOCUMENT CONTROL DATA

1. PRIVACY MARKING / CAVEAT (OF DOCUMENT)

2. TITLE

Simulation of Flow Past a Sphere using the Fluent Code

3. SECURITY CLASSIFICATION (FOR UNCLASSIFIED REPORTS THAT ARE LIMITED RELEASE USE (L) NEXT TO DOCUMENT CLASSIFICATION)

Document	(U)
Title	(U)
Abstract	(U)

4. AUTHOR(S)

D.A. Jones and D.B. Clarke

5. CORPORATE AUTHOR

DSTO Defence Science and Technology Organisation
506 Lorimer St
Fishermans Bend Victoria 3207 Australia

6a. DSTO NUMBER	6b. AR NUMBER	6c. TYPE OF REPORT	7. DOCUMENT DATE
DSTO-TR-2232	AR-014-365	Technical Report	December 2008

8. FILE NUMBER	9. TASK NUMBER	10. TASK SPONSOR	11. NO. OF PAGES	12. NO. OF REFERENCES
2007 / 1110707 / 1	NAV 07 / 119	CANSG	29	54

13. URL on the World Wide Web

http: / / www.dsto.defence.gov.au / corporate / reports / DSTO-TR-2232.pdf

14. RELEASE AUTHORITY

Chief, Maritime Platforms Division

15. SECONDARY RELEASE STATEMENT OF THIS DOCUMENT

Approved for public release

OVERSEAS ENQUIRIES OUTSIDE STATED LIMITATIONS SHOULD BE REFERRED THROUGH DOCUMENT EXCHANGE, PO BOX 1500, EDINBURGH, SA 5111

16. DELIBERATE ANNOUNCEMENT

No Limitations

17. CITATION IN OTHER DOCUMENTS Yes

18. DSTO RESEARCH LIBRARY THESAURUS http: / / web-vic.dsto.defence.gov.au / workareas / library / resources / dsto_thesaurus.shtml

Computational Fluid Dynamics, Numerical Simulation, Fluid Flow, Turbulence

19. ABSTRACT

We use the commercial computational fluid dynamics code Fluent to simulate the flow around a sphere in several different flow regimes; steady-state laminar flow at a Reynolds number (Re) of 100, time-dependent laminar flow at Re = 300, and turbulent flow at $Re = 10^4$ and $Re = 10^6$. These simulations provide a test of the ability of the code to accurately reproduce typical flow structures observed in generic bluff body flows, such as those experienced by submarines and Unmanned Underwater Vehicles (UUVs). The simulations are compared both with experimental results and computations from other computer codes and it is found that Fluent is able to accurately simulate the fluid behaviour in each of the above flow regimes.